Modelling and Simulation in Materials Science and Engineering

Coupled experimental-computational analysis of primary static recrystallization in low carbon steel

OPEN ACCESS
IOP Publishing
Modelling and Simulation in Materials Science and Engineering
Modelling Simul. Mater. Sci. Eng. **28** (2020) 014001 (19pp) https://doi.org/10.1088/1361-651X/ab51bd

Coupled experimental-computational analysis of primary static recrystallization in low carbon steel

Martin Diehl and Markus Kühbach

Max-Planck-Institut für Eisenforschung GmbH, Max-Planck-Str. 1, D-40237 Düsseldorf, Germany

E-mail: m.diehl@mpie.de

Received 28 February 2019, revised 8 October 2019
Accepted for publication 28 October 2019
Published 13 November 2019

Abstract

Primary static recrystallization is a restoration process during which the critically strong deformed microstructure is atomistically reconstructed into a polycrystal with orders of magnitude lower defect density. Advances in diffraction methods catalyzed research activities directed towards more accurate understanding of recrystallization. While these efforts rendered most mechanisms by now qualitatively well understood, many quantitative details remain still unknown. Computer simulations are a viable option to provide qualitative insights into the complex recrystallization process as they provide unlimited observability. However, simulation tools for studying recrystallization in volumes that are significantly large enough for making predictions of mean-field descriptors, such as the distribution of grain sizes or texture evolution, are typically based on continuum models. The use of such models requires to accept certain assumptions on how the collective behavior of multiple thousands of atoms can be homogenized. One aspect of special importance for continuum models is the correct prediction of the nucleation process as it influences virtually all quantitative descriptors of the recrystallized microstructure. This study presents a one-to-one comparison of simulation results to quasi *in situ* scanning electron microcopy/electron backscatter diffraction results revealing how two different assumptions for the crystallographic orientation of the nuclei perform in reproducing the experimentally observed recrystallization microstructure. Moreover, by comparing the recrystallized microstructure at the surface and in the interior of the

three-dimensional model, it is shown how quasi *in situ* experiments systematically underestimate the recrystallization rate and predict a distorted grain size distribution.

Keywords: primary static recrystallization, cellular automata, low carbon steel, nucleation, SEM/EBSD

(Some figures may appear in colour only in the online journal)

1. Introduction

Primary static recrystallization is a restoration process during which the critically strong deformed microstructure is atomistically reconstructed into a polycrystal with orders of magnitude lower crystal defect density [1, 2]. It is a process of fundamental industrial relevance for processing metallic alloys as it allows engineers to tune strength and ductility by controlling grain size and crystallographic texture [3]. This explains the extensive research efforts to characterize the evolution of recrystallization microstructures experimentally [3–6] and use of this knowledge for the design of computer models to simulate this process [7–13]. Collectively, these studies contributed to a quantitative understanding how the crystallographic texture, the stored elastic energy, i.e. dislocation density, and processes such as grain fragmentation influence the evolution of a recrystallizing microstructure. Volume transformation kinetics, texture evolution [14–16], and the evolution of the mean grain size are the descriptors most frequently used to characterize the recrystallization process. While experimental and computational studies rendered most mechanisms by now qualitatively well understood, they also document that many quantitative details remain still inaccurate, thereby posing open questions for further research. An increase in prediction quality from continuum scale simulations can be expected from (1) improved predictions for the nucleation process, i.e. the spatial location and crystallographic location of nuclei and their number density per volume and from (2) more accurate models for grain boundary mobility including e.g. the inclination angle and grain boundary character [17].

In particular the advances in diffraction methods in the last two decades catalyzed research activities towards a more accurate and quantitative understanding of recrystallization. To this end, two main types of experiments have been performed: either metallographically prepared surface regions have been probed in two dimensions using high-resolution scanning electron microcopy/electron backscatter diffraction (SEM/EBSD) [18–24] or the specimens have been measured in three dimensions with hard x-ray radiation to reconstruct from the diffraction signal a synthetic proxy of the polycrystal [13, 25–30]. Strictly speaking, both setups probe only quasi *in situ*, i.e. they provide a sequence of measurements at discrete time steps. This is primarily because—even with the most brilliant sources—measuring statistically relevant areas or volumes at sub-micron resolution demands for orders of magnitude longer acquisition times than it takes the material to recrystallize at typical and especially the industrial relevant annealing temperatures. Despite these limitations, both techniques contributed a to substantial more detailed view of the process, and thereby support simulation efforts either through mechanism identification or by allowing for one-to-one comparison to a ground truth.

It was the advent of efficient computing architectures which made possible the formulation and use of three-dimensional computer models and comparisons of these results with those from experiments. Models which are able to simulate recrystallization in volumes large enough to predict significantly accurate and precise mean-field descriptor values,

though, are typically continuum models, i.e. they are based on certain assumptions how the collective behavior of multiple thousands of atoms can be homogenized. These models evolve a polycrystalline microstructure by tracking the motion of the grain boundary faces through a spatial field of continuum scale dislocation density. Nowadays, a portfolio of solver types and model formulations is available. These solvers have been successfully used for computational studies of recrystallization [7–11, 31]. Reviewing this literature in detail, though, identifies that one-to-one comparisons of an experiment with computer simulations have not performed as often as expected [32–34]. The absence of direct comparisons between full three-dimensional observations—which have been successfully reported for the case of grain growth [35, 36]—can be explained by the challenging microstructural features to resolve, i.e. (sub-) micron sub-grain sizes in conjunction with a high dislocation density.

In the case of comparing surface observations to two- or three-dimensional simulations [24, 37, 38], the differences of the situation at the free surface and in the bulk of the materials needs to be considered to avoid misleading conclusions. More precisely, a strong bias is introduced for instance when comparing the quasi *in situ* experimental kinetics on the specimen surface to a two- or three-dimensional simulation which uses periodic boundary conditions on the computational domain.

In this study we use data from quasi *in situ* SEM/EBSD surface measurements as the input for three-dimensional computer simulations with a cellular automata (CA) model. By comparing the experimentally observable features at the surface to the bulk situation in the simulation, we investigate how the free surface in the experiment influences recrystallization kinetics, grain size distribution, and texture evolution. We lay a special focus on the question how different assumptions for the crystallographic orientation of the nuclei enable us to increase the match between simulation and experiment. The direct comparison to the experimental data allows us to develop and improve our understanding under which circumstances potential nuclei transform into a growing grain. This knowledge can be used in the future to tackle one of the remaining challenges for continuum modeling of recrystallization, namely the formulation of sub-models for the nucleation process. We emphasize that the requirement for a separate formulation of a nucleation model is a direct consequence of the fact that all continuum annealing microstructure evolution models are essentially growth models. Hence, our findings are not only of relevance for simulation tools based on the CA approach but can be used for all other continuum models for primary static recrystallization.

2. Simulation setup

2.1. CA approach

The simulation results in this study were computed with a CA model for primary static recrystallization. CA formulations are—in contrast to other solution techniques—not derived from a (partial) differential equation for which the solution to a boundary or initial value problem is sought numerically. Instead, local evolution rules are defined that can be independently evaluated. While this allows for a straightforward parallelization and associated computationally efficient algorithms, for general cases it is difficult to prove that a CA model follows fundamental physical laws such as energy minimization. However, since the grain boundary energy is neglected in the current model, the total energy is strictly decreasing over time. Like most other continuum models, a CA requires the discretized definition of an initial microstructure. This structure is evolved via integrating the equations of motion for the grain boundary network based on a number of physical sub-models which depend on adjustable constitutive parameters. Specifically, a Statistical Cellular Operator for Recrystallization

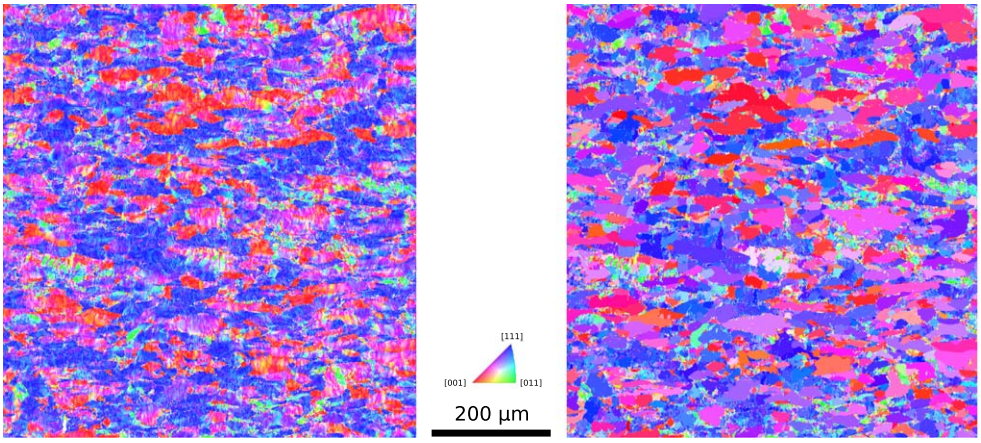

Figure 1. Inverse pole figure (IPF) maps parallel to the normal/out-of-plane direction of the measured deformation microstructure. Horizontal is the rolling direction (RD) and vertical is the transverse direction (TD) in the preceding cold rolling process. The left figure shows the IPF from the as-measured orientation and the right figure shows the IPF resulting from the segmentation process which was used to build the CA model.

(SCORE) model, a real time scaled three-dimensional CA with Moore neighborhood rules and software parallelization [31, 39, 40], was used. Latter allows for fast execution of simulations with multiple billion voxels to gain statistically relevant insights into the process of recrystallization.

2.2. Initial microstructure

The simulations are based on a quasi *in situ* SEM/EBSD annealing experiment of a 65% cold-rolled DC04 low carbon steel [41]. In this experiment, a region perpendicular to the normal direction (ND) of the sheet with size approximately $700 \times 700\,\mu$m was repeatedly probed to track the recrystallization process. The initial microstructure map of dimensions 2761×2801 pixels was measured with a step size of $0.25\,\mu$m and used as input for the CA model, see figure 1. The experimental result was converted into a synthetic initial microstructure using the following protocol: firstly, the data was cleaned using common filters from the TSL OIM software like *neighbor orientation correlation*, *neighbor confidence index correlation*, and *dilatation*. As the next step, the kernel average misorientation (KAM) was computed at each material point using a nearest neighbor kernel with 5° cut-off. As an approximate measure of crystallographic misorientation/lattice curvature, the KAM provides a lower bound for the density of geometrically necessary dislocations (GND) [42, 43]. Next, the grains were segmented using the Matlab MTEX texture toolbox [44, 45]. Given that the sub-grain boundary/dislocation wall network should be identified, a low threshold angle of 2° was used. To avoid artifacts resulting from the finite spatial and angular resolution (right image in figure 2), all grains of this initial segmentation that contained less than 9 pixels were removed, and the segmentation repeated. In a next step, this segmentation was used to calculate the average KAM value per sub-grain, see left image in figure 2. Next, GND values per sub-grain ρ_g were estimated from these averaged KAM values.

Following [46, 47],

$$\rho_g = 3\Omega/(b\Delta) \tag{1}$$

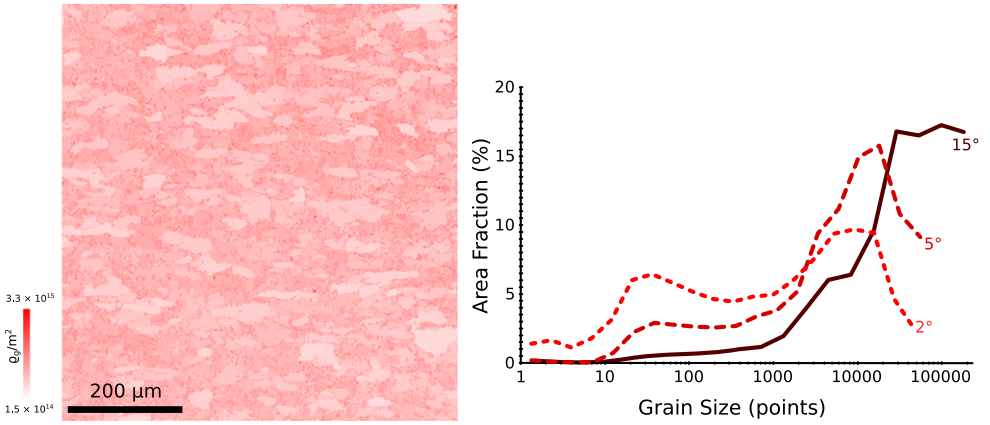

Figure 2. Left figure: density of geometrically necessary dislocations (GND) estimated from the kernel average misorientation (KAM) values obtained for a maximum misorientation angle of 5° averaged over sub-grains segmented using a 2° threshold value. Coordinate system follows figure 1. Right figure: grain size distributions resulting from the threshold values used for the segmentation process (2° and 5°) in comparison to a value for a high-angle grain boundary (12°).

was used here, wherein b is the magnitude of the Burgers vector, Δ the step size, and Ω the KAM value in radians. Recovery of the dislocation density was assumed to be negligible in the considered body-centered cubic (bcc) material [41] during the growth of new grains. Hence, the dislocation in the deformed microstructure remained constant throughout the simulation.

Extending all grains of this two-dimensional microstructure into columns completed the microstructure instantiation. Thereby, a volume element of size $690.5 \times 700.25 \times 25\ \mu$m was discretized into a representative volume element (RVE) of $2761 \times 2801 \times 100$ voxels.

2.3. Boundary conditions

To reflect the situation in the bulk of the material, periodic boundary conditions were applied on the edges of the observation plane. In agreement with the situation in the *in situ* experiment, open boundary conditions were assigned for the top and the bottom RVE domain wall. This allows to monitor two surface planes where the nuclei grow under equal geometrical constraints as they did in the surface characterized in the experiment.

2.4. Nucleation model

Given that the CA—like phase field models, vertex trackers, and level set solvers—is a growth model, a separate (sub-) model for nucleation is required to define the simulation procedure. More specifically, the spatial position, crystallographic orientation, and temporal activation sequence of each individual nucleus needs to be specified. As outlined by [48], the comparable low driving force and the high interface energy between the recrystallized and non-recrystallized region requires large nuclei with approximately 10^{10} atoms. Therefore, 'nucleation' in primary static recrystallizing cannot occur from random fluctuations as it is, for instance, the case in a solidification process. The term 'nucleation' in the context of recrystallization is rather used to denote the process by which a 'candidate nuclei' makes the transition into a persistently growing grain. It should be noted that there is a significant

surplus of potential nucleation sites, i.e. sub-grains, in a heavily deformed microstructure. Only at a fraction of these sites, though, the environment allows the nuclei to make the transition into an actually growing grain [49–51]. Due to this strong selectivity the nucleation process is frequently described as a form of an abnormal growth process which takes place at the sub-grain scale [50, 52]. This is, however, a very phenomenological comparison because —in contrast to abnormal grain growth—many nuclei evolve because of specific mechanistic interactions of grain boundaries with dislocation walls. Moreover, the physical mechanisms are not necessarily comparable to migration during curvature-driven motion in an almost defect free grain. Correctly predicting nucleation therefore requires to identify those microstructural features which make the transition from potential nuclei into new grains favorable. Such features are typically defect less regions that are separated by a mobile, i.e. high-angle grain boundary from the heavily deformed surrounding. This favorable situation, however, does not have to exist in the initial microstructure. At the sub-micron scale, at which nucleation takes place, it could well be that recovery processes at elevated temperatures lead to the formation of new boundaries which encircle virtually defect free volumes.

In the absence of a generally accepted criterion for the determination of nuclei positions in heavily deformed steels, the nuclei were placed in a complete spatial randomness (CSR) [53] process within the microstructure. No incubation time was assumed, i.e. all nuclei were able to grow right from the beginning of the simulation. Two assumptions for the crystallographic orientation of the nuclei were made and compared with respect to their ability to reproduce the experimental results:

1. *Random orientation.* The orientations were sampled randomly from the space of rotations in three dimensions SO(3).
2. *Orientation inheritance.* The nuclei inherited the orientation from the deformed host grain at their respective locations.

The first assumption could be rationalized as follows: sub-grains or grain fragments with a high-angle grain boundary exist in most places of the probed microstructure but their exact position is unknown because of the insufficient spatial resolution of 0.25 μm [49]. Due to the high mobility of these sub-grain boundaries, they are intuitively expected to be the most efficient nuclei for recrystallization. The second assumption could be rationalized as follows: successful nuclei are preferentially located at high-angle grain boundaries and these high-angle grain boundaries can be detected by the SEM/EBSD measurements. When the nuclei inherit the crystallographic orientation of their parents, those nuclei in close proximity to a high-angle grain boundary between two deformed grains are favored over nuclei in the interior of the deformed grains. In fact, the first environment offers a nucleus a mobile grain boundary. In such a situation, growth only depends on the dislocation density in the neighboring grain and, hence, nucleation sites are clustered in regions of high orientation gradients [54].

To our knowledge no general and accurate *a priori* model exists for a precise prediction of the nuclei number density, their number was fitted to the experimental results in a preliminary parameter study. To this end, the number of nucleation sites was independently varied for both nucleation models such that the *mean* grain area of 30 μm^2 measured in the experiment was reproduced. This procedure resulted in 0.22 μm^{-3} nuclei when assuming a random orientation and 0.32 μm^{-3} when assuming orientation inheritance. For the simulated volume this corresponds approximately[1] to 42 000 and 60 000 nuclei, respectively.

[1] The exact number of nuclei depends on the CSR seeding process as one site can be occupied only by one nucleus.

2.5. Mobility model

In SCORE, the mobility m of migrating grain boundaries is modeled according to classical thermal activation theory [55]. For simplicity—and in the absence of more accurate models for primary static recrystallization in bcc metals that are generally accepted and parameterized—it is assumed that $m(\Theta)$ depends exclusively on the disorientation angle Θ:

$$m(\Theta) = c_1 \cdot \left[1.0 - c_2 \cdot \exp\left(-c_3 \cdot \left(\frac{\Theta}{\Theta_c}\right)^{c_4}\right)\right], \tag{2}$$

where Θ_c is threshold disorientation angle and c_1, c_2, c_3, and c_4 are fitting parameters. This functional form reflects two experimental observations: firstly, low-angle grain boundaries migrate orders of magnitude slower than high-angle grain boundaries and secondly, there exists a transition region between 10° and 15° disorientation where mobility increases substantially. Further observations, such as the high mobility of the high-angle grain boundaries with specific bicrystals symmetries or the additional influence of the grain boundary plane normal on the mobility are not considered in this model. Under the simplifying assumption of negligible capillary driving forces and considering the recrystallizing grains as dislocation free, this mobility model allows to compute the grain boundary migration speed $v(\Theta, T, \rho)$ as

$$v(\Theta, T, \rho) = m(\Theta) \exp\left(-\frac{H_\mathrm{m}}{k_\mathrm{B} T(t)}\right) \frac{1}{2} G b^2 \rho \tag{3}$$

in dependence of dislocation density ρ, absolute temperature T, and grain boundary misorientation angle. Based on the assumption that the (measurable) GND density correlates with the total dislocation density, which includes GNDs and statistically stored dislocations, $\rho \propto \rho_\mathrm{g}$ was presumed here. Constitutive parameters are the shear modulus G, the magnitude of the Burgers vector b, and the activation enthalpy H_m. Lastly, k_B is the Boltzmann constant.

2.6. Constitutive parameters

While equations (2) and (3) are simple and lucid, the strong nonlinear dependence of the grain boundary migration speed v on the activation enthalpy H_m imposes severe challenges when obtaining material specific parameters [56]. Since—to the best of the authors' knowledge—no experimental assessment for DC04 has been performed, data for Fe-3.5%Si from [57] were used. Based on the average of the collected and measured data for the activation enthalpy, $H_\mathrm{m} = 2.5725$ eV was chosen. The parameters for the grain boundary mobility, equation (2), were selected as $c_1 = 300\ \mathrm{m^4\ J^{-1}\ s^{-1}}$, $c_2 = 0.9$, $c_3 = 5.0$, $c_4 = 9.0$, and $\Theta_c = 15°$, i.e. grain boundaries with a disorientation angle larger than 15° have a virtually constant mobility of $c_1 = 300\ \mathrm{m^4\ J^{-1}\ s^{-1}}$. Values for shear modulus ($G = 82$ GPa at room temperature) and Burgers vector ($b = 248.5$ pm) for α-iron from experiments by [58] and [59], respectively, have been used.

2.7. Temperature–time profile

The simulated annealing temperature–time profile was taken from the experiment in simplified form, i.e. it follows the nominal profile rather than the measured one. Hence, the temperature $T(t)$ in equation (3) was repeatedly increased from room temperature to 600°C with a heating rate of $100\ \mathrm{K\ s^{-1}}$ and decreased after a holding time with a rate of $200\ \mathrm{K\ s^{-1}}$. The holding time for the first two cycles was 5 and 10 s for the third and last heating cycle. An

adaptive Euler forward integration scheme was used to evolve the cell states. The time step integration along the non-isothermal annealing schedule was controlled with 1 K accuracy. Further details to the numerical procedures are documented elsewhere [31, 60].

3. Results

In total, six simulations have been performed for each of the two nucleation assumptions in which the spatial position of the nuclei follows a different random distribution. Taking the top and bottom section of the RVE into account for evaluation, this gives twelve microstructure maps that can be directly compared to the experimental results for each case. Comparison of these results shows that the statistical ensemble of the nuclei and the deformation texture is representative for the considered material. More precisely, the scatter in the recrystallization kinetics and the grain size distribution among the realizations is less than 2%. For this reason, in the following results are mostly discussed on the basis of one realization only.

For an unbiased comparison to the experimental results, the procedure for evaluating the results of the computer simulations mimics the two main limitations when processing the experimental data: (1) to mirror the two-dimensional experimental setup, each section parallel to the experimental observation plane of the three-dimensional simulation volume is analyzed independently. (2) To account for the uncertainties when detecting new grains based on KAM values, only grains that contain at least 13 points (equivalent to an area of 0.8 μm^2) are considered. These surface sectioning analyses were executed after every integration step. As shown later on, following this procedure is essential for the correct comparison of experimentally and computationally obtained quantities.

3.1. Global recrystallization kinetics

The overall recrystallization kinetics, i.e. the recrystallized area fraction X_A over time is shown in figure 3(a) for the case of an inherited crystallographic orientation and for the case of random sampling from the SO(3) separately for the top/surface plane and for the central plane. The experimental data is also given in this figure. It can be seen that both choices—how deeply is the observation plane embedded in the bulk and which crystallographic orientation was assigned to the nuclei—have a strong influence on the apparent recrystallization rate: recrystallization in the bulk occurs faster than on the surface and random sampling of the nuclei orientation gives a higher recrystallization rate than the assumption of orientation inheritance. As shown in [41], also the experimentally observed values for X_A scatter significantly: after nominally the same time at peak temperature 600°C, X_A varied from 4% to 35% for $t = 5$ s, 10% to 50% for $t = 10$ s, and 32% to 65% for $t = 20$ s. The upper limits measured by [41] are given together with the values for the microstructure used here as the simulation. It should be noted that this microstructure had one slowest kinetics that were experimentally observed.

All simulation results predict faster kinetics than observed experimentally (indicated by a bold X) and even exceed the maximum values among all probed samples of the same material (indicated by normal font x) for nominal annealing times of 10 and 20 s. While, on the one hand, this is a result of the adjustment of the number of nucleation sites to the experimentally observed grain size distribution, control simulations with an enthalpy H_m increased by only 3% resulted in a decrease of the recrystallization rate such that the experimentally observed value of $X_A = 46\%$ for $t = 20$ s was not reached. It should be noted that such a small decrease lies well within the error margins reported by [57]. Given this strong influence of the parametrization on the overall model behavior, it becomes immediately clear that specifying

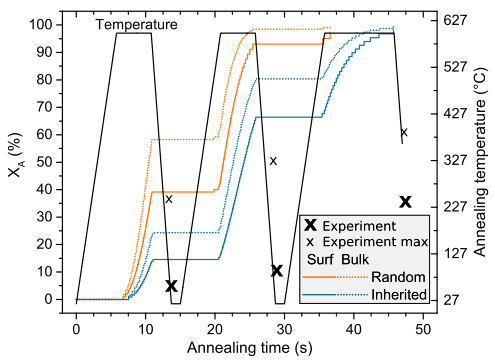

(a) Evolution of the recrystallized area fraction X_A and temperature over time. The computational results are compared to the experimental data from Diehl *et al* [41].

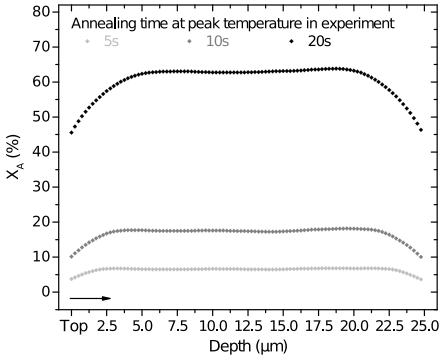

(b) Evolution of the recrystallized area fraction X_A for $X_A(z = 0) \in (4\%, 10\%, 46\%)$ through the thickness of the volume element.

Figure 3. Recrystallization kinetics in comparison to the experimental results.

further detailed grain boundary mobility or energy landscape models without improving their parameterization based on insights from experiments or atomistic simulations will not increase the quality of the simulation. Therefore, as extensive parameter fitting was not the aim of this study and the details of the recrystallization kinetics are not of importance for the further investigation, no further tuning of the parameters was performed.

Figure 3(b) shows the profile of the $X_A \in (4\%, 10\%, 46\%)$ over the depth of the simulation volume. This correspond to $t \in (5\ \text{s}, 10\ \text{s}, 20\ \text{s})$ of nominal annealing time at peak temperature 600°C in the experiment. This figure confirms the observation of significantly faster kinetics in the bulk than at the surface. Moreover, the smooth and symmetric curve clearly indicates that the measured plane is representative for the microstructure, i.e. it contains a sufficient ensemble of recrystallizing grains to infer kinetics from.

3.2. Recrystallization microstructure

Figure 4 shows inverse pole figure (IPF) parallel to the ND, which is also the normal of the observation plane. Only recrystallized grains are shown. For comparison, the IPFs are shown for the same recrystallized area fraction of $X_A = 46\%$. This corresponds, as obvious from figure 3(a), to different annealing times. The experimental result (center) is compared to the case of random orientation assignment (left) and orientation inheritance (right). The top row gives the results from a central plane (bulk behavior) and the bottom row gives results from one of the outer planes (free surface). Significant differences between the two nucleation models can be seen: spatially, the distribution of new grains is more homogeneous when assuming a random orientation assignment than in the case of orientation inheritance. With respect to the crystallographic orientation, the expected trends are observed: random seeding results in a rather 'colorful' IPF map, indicating also a random orientation of the recrystallized grains, i.e. no growth selection seems to take place. In the case of the orientation inheritance, grains colored in red and blue are seen more often. This reveals that orientations having the $\langle 001 \rangle$ and $\langle 111 \rangle$ direction aligned with ND dominate the recrystallization texture. These are the orientations that are also seen frequently in the deformation microstructure, see figure 1.

Qualitatively, the more heterogeneous spatial distribution of the recrystallizing grains that is obtained in the case of orientation inheritance matches closer the experimental results. However, the heterogeneity observed experimentally is much stronger. In contrast, when

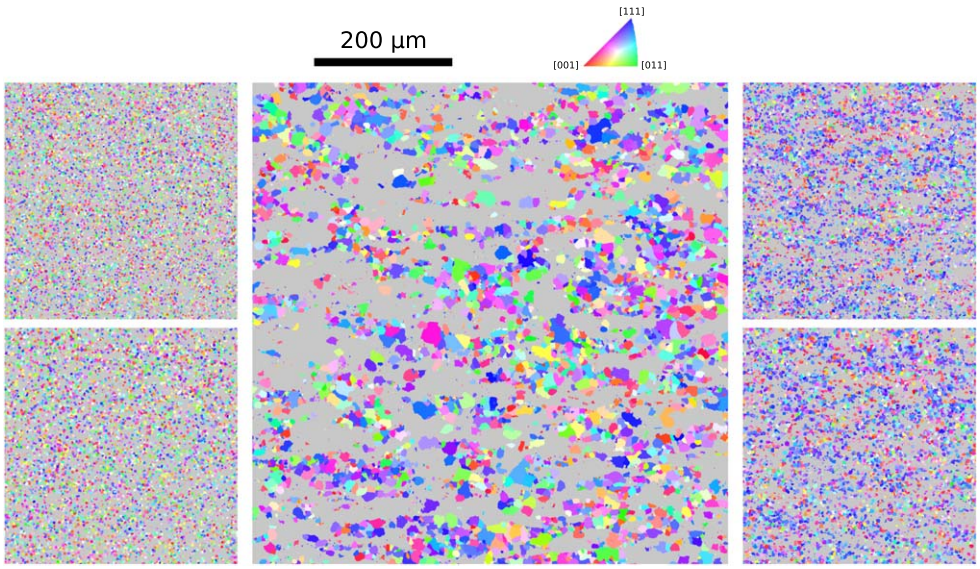

Figure 4. Inverse pole figure (IPF) map parallel to the normal direction/observation plane of the recrystallized grains. The central figure shows the experimental result. The left pair of figures show the results for the assumption of randomly oriented nuclei. The right pair of figures for orientation inheritance where the top figures are results from the central plane and the bottom figures from a surface plane. Note that (1) the simulation results are scaled to one quarter of the area and that (2) a slight misalignment between the experimental results (obtained after 20 s of annealing) and the simulation results (based on the measurement before the heat treatment) exists.

comparing the the crystallographic orientations, no clear preference for either nucleation assumption can be drawn: the orientations seen in the experiment seem to consist of a mixture of 'inherited' and 'random'. It can be also seen that larger grains, which are observed in the experiment, are totally absent in both simulation results. Yet, a slightly more heterogeneous grain size distribution can be observed for the assumption of orientation inheritance, which is even more pronounced when looking at the surface plane.

3.3. Grain size distribution

The mean and median values of the measured grain area are given in table 1 for $X_A = 46\%$, i.e. again for different annealing times. It can be seen that the grains at the surface are larger than in the bulk of the material. Moreover, while the median is significantly smaller for the experimentally observed distribution than the mean, both measures take essentially the same values in all simulation results.

For a more detailed analysis, the experimentally observed grain area distribution for $X_A = 46\%$ is shown together with the results for the considered four cases (random orientation versus orientation inheritance and free surface versus bulk observation) in figure 5. In this figure, the cumulative distribution of grains that have a specific area in the observation plane is plotted. It is obvious that, despite adjusting the model parameters to obtain a similar mean value, both seeding methods do not result in grain size distributions which match the experimental results. More specifically, the CA simulations predict a much narrower grain size distribution: large grains, which are observed in the experiment, are not predicted by the

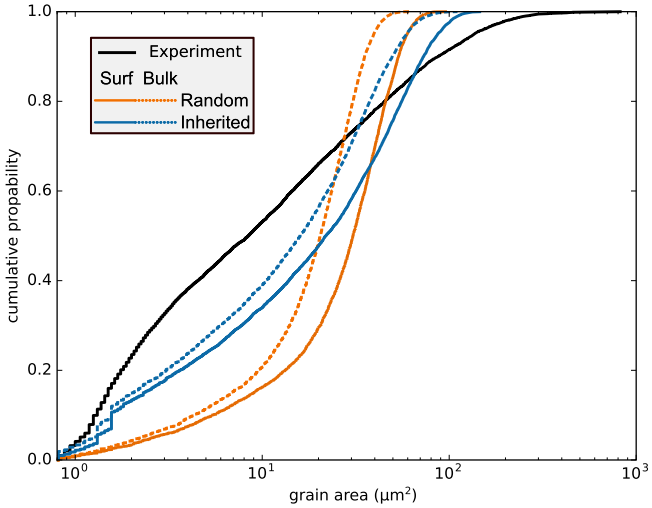

Figure 5. Grain size distribution in terms of the area for an recrystallized area fraction of $X_A = 46\%$. The cumulative probability is based on the number of counts for grains with a given area.

Table 1. Mean and median values of the grain area (in μm^2) measured for different sectioning planes perpendicular to the observation direction for an recrystallized area fraction of $X_A = 46\%$. Note that this grain area is not directly scalable into a grain diameter owing to stereological reasons.

	Mean	Median
Experiment	30	8
Random sampling in the bulk	21	20
Random sampling at the surface	30	31
Orientation inheritance in the bulk	21	15
Orientation inheritance at the surface	31	22

simulations at all and the number of small grains in the simulations is significantly underestimated compared to the experiment. While this observation is true for all considered cases, comparing the simulation results to each other reveals that a better match is obtained for the case of orientation inheritance. Moreover, the simulation results obtained at the surface are in better agreement to the experimental result—also obtained on the surface—than are their counterparts from within the bulk.

3.4. Recrystallization texture

The recrystallization texture in terms of (difference) pole figures is shown in figure 6. These figures are obtained from orientation distribution functions calculated with MTEX using a de La Valle Poussin kernel with a half width of 10°. The results shown here are collected from the combined data from all surface planes for the respective nucleation assumption. No results from the bulk planes are shown as no texture difference was observed. The quantitative results visible in figure 4 are confirmed qualitatively: the assumption of random orientation

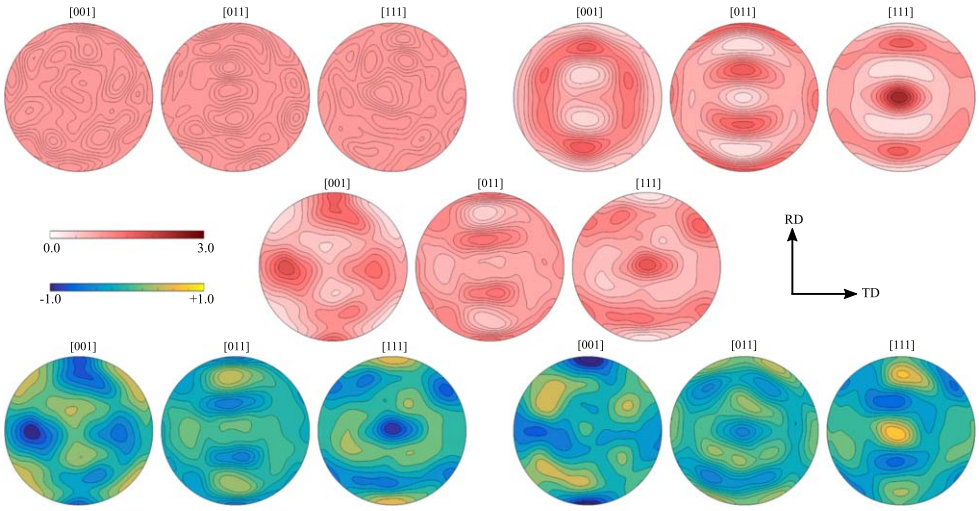

Figure 6. Pole figures computed from orientation distribution functions (ODF) of the simulation results (top row) and the experimental results (middle row) together with the difference pole figures between them (bottom row). The simulation results for random nucleation and orientation inheritance are shown in the left and right column, respectively. The simulation results are obtained from the combined data of all surface layers. RD: rolling direction, TD: transverse direction.

for the nuclei results in an essentially random orientation, i.e. there is also no particular orientation preferred during the growth of the grains. The assumption of orientation inheritance is qualitatively closer to the experimental results but overestimates the texture. More specifically, the ⟨111⟩ directions appear too frequently and the ⟨110⟩ direction aligned with the rolling direction is underestimated significantly.

3.5. Site-specific recrystallization probability

Whether a specific location in the microstructure is expected to recrystallize, we computed the recrystallization probability from the combined information of all 12 surface planes. Specifically, this probability was computed as the mean of the two states 'deformed' and 'recrystallized' where the former is represented by a value of 0.0 and the latter by a value of 1.0. When mapping these values on a gray color bar, the points that have been recrystallized in all of the twelve realizations appear in black color and the points which have not recrystallized in any of the realizations are shown in white color. Figure 7 shows this measure for the case of orientation inheritance (left) and random nucleation (right). These results are compared to the experimentally observed recrystallization microstructure at $X_A = 46\%$, i.e. the one after nominally 20s holding time at peak temperature 600°C. In the experiment, a clear correlation between GND density and the local recrystallization was observed [41], i.e. the black regions in figure 7 (center) correspond to regions of high stored energy. Both simulations reproduce the experimentally observed spatial inhomogeneity to some extent, where the separation into regions with a high respectively low recrystallization tendency is more pronounced when assuming an inherited crystallographic orientation for the nuclei. In agreement with the experiment, regions of low recrystallization probability are regions with a low GND density. Even though no perfect spatial correspondence between experimental result (measured after three heating cycles) and simulation results (based on the measurement

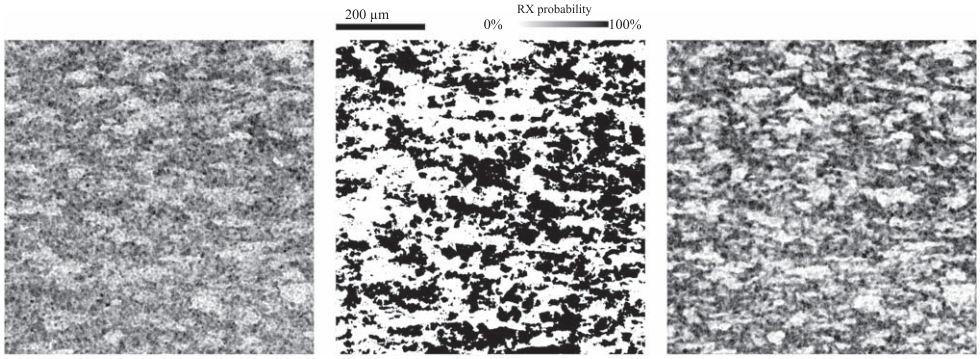

Figure 7. Spatial distribution of the recrystallized microstructure for $X_A = 46\%$. In the experimental result (center, after 20 s at 600°C) recrystallized areas are given in black and the remaining deformation microstructure in white. The simulation results at the surface plane are obtained as the average over twelve planes for the case of random orientation (left) and orientation inheritance (right), respectively.

of the deformation microstructure) exists, some features from the experimental characterization are reproduced by the simulations.

4. Discussion

The presented one-on-one comparison of experimentally measured and simulated primary static recrystallization reveals deviations which pinpoint important consequences for the evaluation of quasi *in situ* experiments based on surface measurements of this process.

With respect to the crystallographic orientation of the nuclei, it can be seen that the assumption of a random orientation gives a far too weak recrystallization texture while letting the nuclei inherit the orientation of the deformed microstructure results in an overly strong texture. As it is accepted, the orientation of the nuclei for recrystallization needs to be inherited from the deformation microstructure, this discrepancy allows to draw the following conclusions: it is necessary to measure the geometry of the deformed microstructure with higher spatial resolution. At the same time, though, this must not compromise area statistics. Exemplified for this study, a five-fold increase of the original resolution would result in approximately 10 days of acquisition time. Retaining stable imaging conditions and avoiding beam-induced damage are substantial challenges for such long acquisition times. In effect, small sub-grains (possibly with a high misorientation) that serve as potentially effective nuclei or affect the evolution of neighboring such, are not present in the initial microstructure representation used as our input to the simulation. The cleaning of the experimental data—which is a common procedure when analyzing EBSD results—additionally contributes to difficulties in detecting highly misoriented sub-grains. This is particularly detrimental for characterizing the grain boundary trace geometry. The latter is relevant to quantify the capillary driving forces, and thereby the population of smaller sub-grain boundary facets, which ought to drive and tune most strongly the capillary driving forces in the incipient nucleation stage. It is this insufficient spatial resolution of the grain boundary trace geometry that forbids to make an accurate assessment of the distribution of projected boundary curvature within the system, or at least renders such assessments qualitative. Second, from the comparison of the grain areas, it can be inferred that the assumption of 'site-saturated' nucleation is not fulfilled in the experiment. Under this assumption, all nuclei with a mobile

grain boundary start to grow immediately and compete with each other. Hence, there are no grains with a time advantage that would allow them to grow significantly faster than others. Third, the requirement to increase the number density of nuclei in the case of orientation inheritance to match the experimentally observed *mean* grain size indicates that a significant number of nuclei cannot grow under the assumption of orientation inheritance because they have no mobile high-angle boundary to the surrounding microstructure. While the assumption of orientation inheritance results in a more realistic, i.e. wider grain size distribution than the assumption of random orientation for the nuclei, the difference to the experimental results remain significant.

The inability to reproduce the experimental results independently of the selected model for the crystallographic orientation of the nuclei clearly indicates that not all relevant physical mechanisms are appropriately described, i.e. not all significant mechanisms were identified and, even more important, all mechanisms were parameterized with accurate and precise values.

In this regard, the present work documents that several improvements on the modeling and parameter identification side are required:

1. *The nucleation model*. While a mixture of both assumptions for the crystallographic orientation investigated in this study most probably would result in a macroscopic texture in reasonable agreement with the experimental findings, such a phenomenological approach can hardly be called a sound, physical-based nucleation model. Hence, the development of nucleation models that make understanding obtained from the consideration of sub-grains ensembles [50, 51] accessible to continuum scale models can be expected to increase the predictive qualities of recrystallization simulations. However, it will demand future studies to assess on an even smaller scale and further detail the local geometry, topology, surplus the dislocation density field situation.
2. *The grain boundary mobility model*. Various models and simulations [17, 61–63] show that the grain boundary mobility depends on details such as disorientation, inclination angle, and, in fact, the detailed atomic mechanisms taking place in its interfacial defect structure and junction network [64]. Still, despite recent efforts [17], this knowledge has not been cast yet into general expressions for continuum models that can be parameterized over the full, five dimensional space required to describe a grain boundary macroscopically. In this context, it should be emphasized that for engineering alloys the feasibility to determine the mobility experimentally [56, 57] remains important because potentials for molecular dynamics (MD) simulations are often not available for complex compositions because accurate potentials do not exist.
3. *The grain morphology model*. Due to the current limitations of 3D characterization techniques [26, 65, 66] in dealing with severely deformed microstructures, *in situ* experiments of recrystallization are out of reach at the moment. While serial sectioning EBSD experiments are destructive in nature, they can at least provide realistic 3D microstructures that allow for comparison of statistical descriptors.
4. *The driving force models.* It should be critically assessed whether two common simplifications for modeling primary static recrystallization are justified: namely, the omission of grain boundary energy anisotropies and capillary driving forces. In the present work, both are excluded. Therefore, the simulation results are likely biased quantitatively compared to experiment. However, without realistic, i.e. 3D sub-grain and deformation microstructural interface geometries, the grain boundaries are not characterized with sufficient precision.

5. *Unraveling of overlapping mechanisms.* Even if above improvements are implemented, a fundamental challenge remains: that is how to disentangle the quantitative contributions from the various mechanisms to arrive at a mechanistic understanding of the incipient stage of nucleus formation and growth. For this task, one-on-one assessments as presented above are useful but should be performed ideally as 4D experiments. For grain growth, the benefits of 4D experiments have been clearly demonstrated by [67].

Despite the shortcomings of the model pointed out above, this study allows to improve the protocols for interpretation of surface-based *in situ* experiments and the comparison of such experiments to simulations. The results here show that inferring kinetics from measurements conducted on free surfaces are an erroneous application of Delesse's principle [68]. Latter states that recrystallized area fractions and volume fractions are equivalent given that the sample is large enough. However, this only holds if the microstructure is characterized *a posteriori* by cutting a bulk specimen open and measuring sections on these samples. For quasi *in situ* studies this is, however, not the case because therein nucleation is confined *a priori* to only one side of the observed plane and, therefore, the evolution of the area fraction measured on the surface diverges from the volume fraction. This has severe practical consequences for the interpretation of results from such studies: while the observed kinetics can still serve as a lower bound estimate, grain size distribution and nuclei number density are not directly accessible from such surface measurements. Care must also be taken when designing simulations to complement experimental investigations [24, 37, 38]. Firstly, it is incorrect in such cases to assume periodic boundary conditions on all surface faces of the computational domains. Secondly, it is quantitatively incorrect to estimate the nuclei number density or calibrate the mobility parameters from corresponding two-dimensional or three-dimensional simulations that are able to reproduce the experimental surface observations. In the case of a two-dimension simulation, the grains are truly confined to the plane while in the case of the *in situ* experiments most nuclei grow from the sub-surface. In the case of a three-dimensional simulation, grains will also evolve differently in comparison to the experiment as nuclei that are visible in a specific observation plane can be located above or below this plane —exactly the same situation as in the bulk of the microstructure.

5. Summary and outlook

In this work, a simulation study is presented that aims at a better understanding of an experimentally observed recrystallization process in a DC04 low carbon steel. Two different assumptions for the orientation of the newly formed grains have been compared. While neither the assumption of random orientation nor the assumption of orientation inheritance allows to reproduce the experimental results with full satisfaction, the latter one results in a better match. More precisely, the recrystallization texture matches the experimentally obtained but is significantly sharper and the grain size distribution shows a closer agreement for larger grains. Despite the simple approach for extending the measured two-dimensional microstructure map into a three-dimensional volume element for the simulation, the results also allow to quantify the limitations of surface-based experiments: quasi *in situ* experiments underestimate the recrystallization kinetics significantly (here by approximately 20% recrystallized volume/area fraction) and predict too wide grain size distributions. These findings are a direct consequence of reducing the number of nuclei by 50% when observing a free surface. Considering in addition their inability to capture the three-dimensional shape of the grains is a strong argument against using such experiments at all to study nucleation quantitatively. With respect to the predictive quality of continuum scale simulations, two

important conclusions can be drawn: First, the high sensitivity of the recrystallization kinetics on the activation enthalpy makes it virtually impossible to reliably predict the evolution of the recrystallized volume or area fraction over time without an experimental base. Consequently, a significant improvement of mean field simulations, specifically the handling of the nucleation criteria, needs to assess in more quantitative detail the effects of nucleation time, spatial locations and correlations, crystallographic orientation, i.e. the detailed three-dimensional deformation microstructure geometry.

Acknowledgments

Christian Broß is acknowledged for preparing and measuring the SEM/EBSD datasets. MD acknowledges the funding of the *TCMPrecipSteel* project by the *Deutsche Forschungsgemeinschaft* in the framework of SPP 1713 *Strong coupling of thermo-chemical and thermo-mechanical states in applied materials*. MK appreciates that the work was partially supported by the Deutsche Forschungsgemeinschaft through project RO 2342/8-1 and partially through *BiGmax*, the *Max-Planck-Society's Research Network on Big-Data-Driven Materials Science*. The discussions with Stefan Zaefferer on the limitations of surface measurements and with Dierk Raabe on the importance of nucleation are gratefully acknowledged.

Work sharing

MD designed the study, conducted analyses, and wrote the manuscript. MK conducted the simulations and contributed to the manuscript through writing parts of it and in-depth discussions.

Data availability

All simulation input and results, including the SCORE source code used to execute this study, is available as supplementary open source material [60].

ORCID iDs

Martin Diehl https://orcid.org/0000-0002-3738-7363
Markus Kühbach https://orcid.org/0000-0002-7117-5196

References

[1] Cahn R W 1996 Recovery And recrystallization *Physical Metallurgy* ed R W Cahn and P Haasen (Amsterdam: North-Holland) pp 2399–500
[2] Doherty R D, Hughes D A, Humphreys F J, Jonas J J, Jensen D J, Kassner M E, King W E, McNelley T R, McQueen H J and Rollett A D 1997 Current issues in recrystallization: a review *Mater. Sci. Eng.* A **238** 219–74
[3] Humphreys J, Rohrer G S and Rollett A 2017 *Recrystallization and Related Annealing Phenomena* 3rd edn (Amsterdam: Elsevier)
[4] Cotterill P and Mould P R 1976 *Recrystallization and Grain Growth in Metals* 1st edn (London: Surrey University Press)
[5] Hässner F 1978 *Recrystallization of Metallic Materials* 2nd edn (Stuttgart: Dr. Riederer Verlag)

[6] Hölscher M, Raabe D and Lücke K 1994 Relationship between rolling textures and shear textures in f.c.c. and b.c.c. metals *Acta Metall. Mater.* **42** 879–86
[7] Rollett A D, Srolovitz D J, Doherty R D and Anderson M P 1989 Computer simulation of recrystallization in non-uniformly deformed metals *Acta Metall.* **37** 627–39
[8] Humphreys F J 1992 Modelling mechanisms and microstructures of recrystallisation *Mater. Sci. Technol.* **8** 135–44
[9] Rollett A D 1997 Overview of modeling and simulation of recrystallization *Prog. Mater. Sci.* **42** 79–99
[10] Raabe D 2002 Cellular automata in materials science with particular reference to recrystallization simulation *Annu. Rev. Mater. Res.* **32** 53–76
[11] Hallberg H 2011 Approaches to modeling of recrystallization *Metals* **1** 16–48
[12] Ilin D N, Bozzolo N, Toulorge T and Bernacki M 2018 Full field modeling of recrystallization: effect of intragranular strain gradients on grain boundary shape and kinetics *Comput. Mater. Sci.* **150** 149–61
[13] Zhang J, Voorhees P W and Poulsen H F 2018 (P1-44) Combining 4D experiments and phase-field modeling to determine reduced grain boundary mobilities *MMM2018 Conf. Proc.*
[14] Barnett M R and Kestens L 1999 Formation of $\{111\}\langle 110\rangle$ and $\{111\}\langle 112\rangle$ textures in cold rolled and annealed IF sheet steel *ISIJ Int.* **39** 923–9
[15] Inamura T, Shimizu R, Kim H Y, Miyazaki S and Hosoda H 2016 Optimum rolling ratio for obtaining $\{001\}\langle 110\rangle$ recrystallization texture in Ti–Nb–Al biomedical shape memory alloy *Mater. Sci. Eng.* C **61** 499–505
[16] Imandoust A, Barrett C D, Oppedal A L, Whittington W R, Paudel Y and El Kadiri H 2017 Nucleation and preferential growth mechanism of recrystallization texture in high purity binary magnesium-rare earth alloys *Acta Mater.* **138** 27–41
[17] Wei C, Thomas S L, Han J, Srolovitz D J and Xiang Y 2019 A continuum multi-disconnection-mode model for grain boundary migration *J. Mech. Phys. Solids* **133** 103731
[18] Hutchinson W B and Ray R K 1973 On the feasibility of in situ observations of recrystallization in the high voltage microscope *Phil. Mag.* **28** 953–60
[19] Le Gall R, Liao G and Saindrenan G 1999 In-situ sem studies of grain boundary migration during recrystallization of cold-rolled nickel *Scr. Mater.* **41** 427–32
[20] Hurley P J and Humphreys F J 2004 A study of recrystallization in single-phase aluminium using *in situ* annealing in the scanning electron microscope *J. Microsc.* **213** 225–34
[21] Van Der Zwaag S, Anselmino E, Miroux A and Prior D J 2006 *In-situ* SEM observations of moving interfaces during recrystallisation *Mater. Sci. Forum* **519–521** 1341–8
[22] Nakamichi H, Humphreys F J and Brough I 2008 Recrystallization phenomena in an IF steel observed by *in situ* EBSD experiments *J. Microsc.* **230** 464–71
[23] Bozzolo N, Jacomet S and Loge R E 2012 Fast *in situ* annealing stage coupled with ebsd: a suitable tool to observe quick recrystallization mechanisms *Mater. Charact.* **70** 28–32
[24] Sukhopar O 2016 Experimental and simulation-supported study of cube grain nucleation based on EBSD investigations *PhD Thesis* RWTH Aachen University, Aachen, Germany
[25] Lauridsen E M, Poulsen H F, Nielsen S F and Jensen D J 2003 Recrystallization kinetics of individual bulk grains in 90% cold-rolled aluminium *Acta Mater.* **51** 4423–35
[26] Poulsen H F 2004 *Three-Dimensional X-Ray Diffraction Microscopy: Mapping Polycrystal and Their Dynamics* (Berlin: Springer)
[27] Zhang Y B, Godfrey A and Jensen D J 2014 In-situ investigation of local boundary migration during recrystallization *Metall. Mater. Trans.* A **45** 2899–905
[28] Lin F, Zhang Y, Poulsen S O, Schell N, Pantleon W and Juul Jensen D 2015 Kinetics of individual grains during recrystallization of cold-rolled copper *IOP Conf. Ser.: Mater. Sci. Eng.* **82**
[29] Zhang J, Morsdorf L and Tasan C C 2016 Multi-probe microstructure tracking during heat treatment without an in situ setup: Case studies on martensitic steel, dual phase steel and β-Ti alloy *Mater. Charact.* **111** 137–46
[30] Zeng Z R, Zhu Y M, Xu S W, Bian M Z, Davies C H J, Birbilis N and Nie J F 2016 Texture evolution during static recrystallization of cold-rolled magnesium alloys *Acta Mater.* **105** 479–94
[31] Kühbach M 2017 Efficient recrystallization microstructure modeling by utilizing parallel computation *PhD Thesis* RWTH Aachen (https://doi.org/10.18154/RWTH-2018-00294)
[32] Rollett A D, Alvi M H and Brahme A P 2003 Recrystallization kinetics in hot rolled aluminum: a combined experimental and simulation approach *Tms Annual Meeting* 269–78

[33] Brahme A P, Fridy J M and Rollett A D 2007 Modeling recrystallization in aluminum using input from experimental observations *Mater. Sci. Forum* **558–559** 1057–61
[34] Brahme A, Fridy J M, Weiland H and Rollett A D 2008 Modeling texture evolution during recrystallization in aluminum *Modell. Simul. Mater. Sci. Eng.* **17** 015005
[35] McKenna I M, Poulsen S O, Lauridsen E M, Ludwig W and Voorhees P W 2014 Grain growth in four dimensions: a comparison between simulation and experiment *Acta Mater.* **78** 125–34
[36] Sun J *et al* 2017 4D study of grain growth in armco iron using laboratory x-ray diffraction contrast tomography *IOP Conf. Ser.: Mater. Sci. Eng.* **219** 012039
[37] Schäfer C 2011 Recrystallization modeling considering second-phase particle *PhD Thesis* RWTH Aachen University, Aachen, Germany
[38] Brüggemann T 2016 Automatisierte prozesskettensimulation mit integrierter mikrostrukture-ntwicklung: am beispiel der thermomechanischen behandlung von aluminiumwerkstoffen *PhD Thesis* RWTH Aachen University Germany
[39] Kühbach M, Gottstein G and Barrales-Mora L A 2016a A statistical ensemble cellular automaton microstructure model for primary recrystallization *Acta Mater.* **107** 366–76
[40] Kühbach M, Gottstein G and Barrales-Mora L A 2016 SCORE—an MPI-parallelized Cellular Automaton Ensemble model for the Simulation of Primary Recrystallization Phenomena in 3D (https://github.com/mkuehbach/SCORE)
[41] Diehl M, Kertsch L, Traka K, Helm D and Raabe D 2019 Site-specific quasi *in situ* investigation of primary static recrystallization in a low carbon steel *Mater. Sci. Eng.* A **755** 295–306
[42] Taheri M, Weiland H and Rollett A 2006 A method of measuring stored energy macroscopically using statistically stored dislocations in commercial purity aluminum *Metall. Mater. Trans.* A **37** 19–25
[43] Kysar J W, Saito Y, Oztop M S, Lee D and Huh W T 2010 Experimental lower bounds on geometrically necessary dislocation density *Int. J. Plast.* **26** 1097–123
[44] Bachmann F, Hielscher R and Schaeben H 2011 Grain detection from 2d and 3d EBSD data–Specification of the MTEX algorithm *Ultramicroscopy* **111** 1720–33
[45] Bachmann F, Hielscher R and Schaeben H 2010 Texture analysis with MTEX–free and open source software toolbox *Solid State Phenom.* **160** 63–8
[46] Liu Q, Jensen D J and Hansen N 1998 Effect of grain orientation on deformation structure in cold-rolled polycrystalline aluminium *Acta Mater.* **46** 5819–38
[47] Godfrey A, Mishin O V and Yu T 2015 Characterization and influence of deformation microstructure heterogeneity on recrystallization *IOP Conf. Ser.: Mater. Sci. Eng.* **89** 012003
[48] Rios P R, Siciliano F Jr, Sandim H R Z, Plaut R L and Padilha A F 2005 Nucleation and growth during recrystallization *Mater. Res.* **8** 225–38
[49] Xu W Q and Ferry M 2010 The study on the nucleation behaviours in IF steel by 3D EBSD tomography *Mater. Sci. Forum* **654–656** 2334–7
[50] Wang S, Holm E A, Suni J, Alvi M H, Kalu P N and Rollett A D 2011 Modeling the recrystallized grain size in single phase materials *Acta Mater.* **59** 3872–82
[51] Latypov M I, Kühbach M, Beyerlein I J, Stinville J-C, Toth L S, Pollock T M and Kalidindi S R 2018 Application of chord length distributions and principal component analysis for quantification and representation of diverse polycrystalline microstructures *Mater. Charact.* **145** 671–85
[52] Marthinsen K, Friis J and Engler O 2013 Modelling time-dependent nucleation of recrystallization in aluminium alloys *Mater. Sci. Forum* **753** 147–52
[53] Shoemake K 1992 *Uniform Random Rotations* (Amsterdam: Elsevier) pp 124–32
[54] Storm S and Juul Jensen D 2009 Effects of clustered nucleation on recrystallization *Scr. Mater.* **60** 477–80
[55] Turnbull D 1951 Theory of grain boundary migration rates *JOM* **3** 661–5
[56] Basu I, Chen M, Loeck M, Al-Samman T and Molodov D A 2016 Determination of grain boundary mobility during recrystallization by statistical evaluation of electron backscatter diffraction measurements *Mater. Charact.* **117** 99–112
[57] Furtkamp M, Gottstein G, Molodov D A, Semenov V N and Shvindlerman L S 1998 Grain boundary migration in Fe–3.5% Si bicrystals with [001] tilt boundaries *Acta Mater.* **46** 4103–10
[58] Ledbetter H M and Reed R P 1973 Elastic properties of metals and alloys: I. Iron, nickel, and iron-nickel alloys *J. Phys. Chem. Ref. Data* **2** 531–618
[59] Esser H and Müller G 1933 Die gitterkonstanten von reinem eisen und eisen-kohlenstoff-legierungen bei temperaturen bis 1100° *Arch. Eisenhüttenwesen* **7** 265–8

[60] Diehl M and Kühbach M 2019 Experimental—computational analysis of nucleation sites for primary static recrystallization *Technical report* Max-Planck-Institut für Eisenforschung, GmbH, Düsseldorf (https://doi.org/10.5281/zenodo.2540525)
[61] Upmanyu M, Hassold G N, Kazaryan A, Holm E A, Wang Y, Patton B and Srolovitz D J 2002 Boundary mobility and energy anisotropy effects on microstructural evolution during grain growth *Interface Sci.* **10** 201–16
[62] Rollett A D, Gottstein G, Shvindlerman L S and Molodov D A 2004 Grain boundary mobility—a brief review *Z. Met.kd.* **95** 226–9
[63] Janssens K G F, Olmsted D, Holm E A, Foiles S M, Plimpton S J and Derlet P M 2006 Computing the mobility of grain boundaries *Nat. Mater.* **5** 124–7
[64] Thomas S L, Wei C, Han J, Xiang Y and Srolovitz D J 2019 Disconnection description of triple-junction motion *PNAS* **116**
[65] Wang L, Li M, Almer J, Bieler T and Barabash R 2013 Microstructural characterization of polycrystalline materials by synchrotron x-rays *Frontiers Mater. Sci.* **7** 156–69
[66] Maire E and Withers P J 2014 Quantitative x-ray tomography *Int. Mater. Rev.* **59** 1–43
[67] Zhang J 2018 Determination of material parameters by comparison of 3D simulations and 3D experiments *PhD Thesis* Department of Physics, Technical University of Denmark (https://orbit.dtu.dk/files/146596256/dtu_phd_thesis_JinZhang.pdf)
[68] Delesse A E O J 1848 Procédé mécanique pour déterminer la composition desroches *Anal. Mines* **13** 379–88